Journal of
Synchrotron
Radiation

ISSN 0909-0495

Received 24 July 2011
Accepted 22 November 2011

Grazing-incidence synchrotron-radiation ^{57}Fe-Mössbauer spectroscopy using a nuclear Bragg monochromator and its application to the study of magnetic thin films

Takaya Mitsui,[a,b]* Ryo Masuda,[a,b] Makoto Seto,[a,b,c] Edi Suharyadi[b,d] and Ko Mibu[b,d]

[a]Japan Atomic Energy Agency, 1-1-1 Kouto, Sayo-cho, Sayo-gun, Hyogo 679-5148, Japan, [b]CREST, Japan Science and Technology Agency, 4-1-8 Honcho, Kawaguchi, Saitama 332-0012, Japan, [c]Research Reactor Institute, Kyoto University, Kumatori, Sennan-gun, Osaka 590-0494, Japan, and [d]Nagoya Institute of Technology, Gokiso-cho, Showa-ku, Nagoya, Aichi 466-8555, Japan. E-mail: taka@spring8.or.jp

Energy-domain grazing-incidence ^{57}Fe-Mössbauer spectroscopy (E-GIMS) with synchrotron radiation (SR) has been developed to study surface and interface structures of thin films. Highly brilliant ^{57}Fe-Mössbauer radiation, filtered from SR by a $^{57}FeBO_3$ single-crystal nuclear Bragg monochromator, allows conventional Mössbauer spectroscopy to be performed for dilute ^{57}Fe in a mirror-like film in any bunch-mode operation of SR. A theoretical and experimental study of the specular reflections from isotope-enriched (^{57}Fe: 95%) and natural-abundance (^{57}Fe: $\sim$2%) iron thin films has been carried out to clarify the basic features of the coherent interference between electronic and nuclear resonant scattering of ^{57}Fe-Mössbauer radiation in thin films. Moreover, a new surface- and interface-sensitive method has been developed by the combination of SR-based E-GIMS and the ^{57}Fe-probe layer technique, which enables us to probe interfacial complex magnetic structures in thin films with atomic-scale depth resolution.

Keywords: Mössbauer spectroscopy; nuclear Bragg scattering; nuclear monochromator; magnetic thin film; grazing incidence; total reflection.

1. Introduction

Magnetic and structural properties of thin films are of great scientific and technological interest nowadays. In particular, complex magnetic structures often found in low-dimensional systems, such as ultra-thin iron films, present a challenge for developing new surface- and interface-sensitive experimental techniques. For example, in the field of X-ray spectroscopy with synchrotron radiation (SR), grazing-incidence (GI) optics has become one of the most popular depth-sensitive methods for the characterization of surface and interface structures in thin films; a well collimated SR source is very suited for the GI measurements, such as in X-ray absorption spectroscopy, X-ray photoelectron spectroscopy, X-ray magnetic circular dichroism *etc.* Grazing-incidence Mössbauer spectroscopy (GIMS), first studied by Bernstein & Campbell (1963), is also an effective tool for studying the microscopic chemical and magnetic properties of thin films and multilayers. Usually, the depth sensitivity of GIMS is determined by the short penetration length of resonant γ-radiation into a sample at angles where specular reflection takes place. As a result, it can yield some worthwhile element-selective and site-specific information through the change of the hyperfine (HF) interactions with high depth resolution, $\sim$1–50 nm thick. Since such a resolution cannot be obtained with conventional schemes of Mössbauer spectroscopy (MS) without GI optics, many basic studies of GIMS have been performed by using radioisotope (RI) sources and isotope-enriched thin films (Bernstein & Campbell, 1963; Irkaev *et al.*, 1993*a*,*b*, 1995; Isaenko *et al.*, 1994; Andreeva *et al.*, 1996). However, the RI-based MS (RIMS) under GI conditions involves considerable experimental difficulties. The main difficulty is the low brightness of Mössbauer radiation owing to the isotropical property of the γ-radiation from RI; there has been no remarkable progress in the practical application of GIMS with RI sources.

In contrast, since the first reports of SR-based MS (SRMS) with GI optics (Kikuta, 1992; Baron *et al.*, 1992), grazing-incidence SRMS (GISRMS) has been developed rapidly; special features of SR, *i.e.* high brilliance, polarization *etc.*, enable us to perform precise GIMS measurements easily.

Generally, there are two kinds of measurement scheme for SRMS. One is the time-domain SRMS (T-SRMS) using nuclear forward scattering (NFS) (Hastings *et al.*, 1991) and the other is the energy-domain SRMS (E-SRMS) using stroboscopic detection (SD) (Callens *et al.*, 2002; Seto *et al.*, 2009). The scattering processes and the information extracted from the spectrum are critically compared between RIMS, E-SRMS and T-SRMS by Planckaert *et al.* (2009). In T-SRMS, the spectrum is recorded as a beating time response of the nuclear ensemble following a short resonant synchrotron pulse. The HF parameters are determined by the theoretical analysis of the quantum beats, whose frequencies are characteristic of the HF structure. Currently T-SRMS is the most established technique. As for the applications of the time-domain GISRMS (T-GISRMS), novel surface-sensitive analysis techniques of the thin film are developed with unprecedented accuracy, which include spin structure imaging, domain size determination using off-specular reflection, layer-selective magnetization measurements with circularly polarized SR X-rays, diffusion and even phonon dynamics on the surface layer of materials (Chumakov *et al.*, 1999; Sladecek *et al.*, 2002; Röhlsberger *et al.*, 2002, 2003; Nagy *et al.*, 2002; L'abbé *et al.*, 2004; Ślęzak *et al.*, 2007*a*,*b*, 2010). There is no doubt that T-GISRMS is extremely useful for advanced GIMS studies. However, the complicated interference pattern of the time spectrum often inhibits the data analysis on the complex materials because a minor change of the sample conditions entirely modifies the T-SRMS spectrum with full time windows. On the other hand, in SD-based E-SRMS, the nuclear ensemble in both an investigated sample and a vibrating reference absorber are collectively excited by the SR pulse. The delayed nuclear resonant scattering is recorded as a function of the velocity of the reference absorber so that the energy-resolved spectrum is obtained like in RIMS. In comparison with T-SRMS, E-SRMS is more convenient for online interpretation of the data because the E-SRMS spectrum shows all excited nuclear transitions in the well resolved resonance lines even for the complex materials (Planckaert *et al.*, 2009). Therefore, E-SRMS has also been used in GISRMS study (Deák *et al.*, 2006). In comparison with RIMS, T-SRMS and SD-based E-SRMS have a different scheme for detecting nuclear resonant scattering signals; such methods depend on the bunch operation modes of SR. For instance, T-GISRMS requires special bunch modes of SR having a rather long period ($T > 100$ ns for ^{57}Fe nuclei) between electron bunches in the storage ring. Unfortunately, such bunch modes are usually limited in SR facilities. Furthermore, the SD-based E-SRMS spectrum is strongly influenced by the observation time window so that the deformed profile prevents us from using the established data analysis techniques of conventional MS. Such restrictions may be still the obstacles for a precise analysis of complicated HF structures in the SRMS spectrum.

As for the study of iron-containing materials, all of the above problems can be solved by E-SRMS using a nuclear Bragg monochromator (NBM). In this method extremely high-brilliant single-line ^{57}Fe-Mössbauer radiation is filtered directly from a SR source by a single-line pure nuclear Bragg reflection from a $^{57}FeBO_3$ crystal near the Néel temperature. As a result, we can perform experiments in the same manner as for RIMS by moving the $^{57}FeBO_3$ single crystal using a velocity transducer (Smirnov *et al.*, 1997; Mitsui *et al.*, 2009).

In this paper we report the first GISRMS studies using a NBM. The coherent interference effects between scatterings from electrons and nuclei and between scatterings from the different nuclear transitions are calculated and they are verified experimentally by energy-domain GISRMS (E-GISRMS) for ^{57}Fe-enriched and non-enriched thin films. As a new monolayer-sensitive method, E-GISRMS combined with the ^{57}Fe-probe layer technique has been developed and applied to characterize the interface of Cr/Fe multilayer thin films; the principle of this proposed method is based on a special feature of E-GISRMS for dilute ^{57}Fe in thin films.

2. Theoretical simulation

This section describes equations on GIMS and calculations based on them. Basic features of the GIMS spectrum are displayed by the simulations of specular reflection from thick mirror-like iron films, containing ^{57}Fe nuclides with magnetically split nuclear levels.

The reflectivity of GIMS is given by the square absolute of the Fresnel formula (Bernstein & Campbell, 1963; Irkaev *et al.*, 1993*a*),

$$R(\theta, E) \cong \left|(\theta - \theta_{\rm d})/(\theta + \theta_{\rm d})\right|^2, \tag{1}$$

where θ and E represent the glancing angle and energy of photons, respectively, and $\theta_{\rm d}$ is the refractive angle, given by

$$\theta_{\rm d} = \left(\theta^2 + \chi_{\rm d}\right)^{1/2}, \tag{2}$$

where $\chi_{\rm d}$ represents the susceptibility of the iron film.

To simplify the calculation we limit the case [see Fig. 1(*a*)] as follows. The incident ^{57}Fe-Mössbauer radiation is linearly polarized in the scattering plane (π-polarization) and the HF magnetic field ($H_{\rm hf}$) is aligned parallel to the magnetic polarization unit vector h_π of the incident radiation. Note that, in the SRMS experiments, such an optical system can be easily assembled by using the linear-polarized SR-^{57}Fe-Mössbauer radiation and an external magnetic field (see Fig. 2). In this condition, only the two nuclear transitions of $\Delta m = 0$ are excited selectively ($\Delta m = m_{\rm e} - m_{\rm g}$, $m_{\rm e}$ is the magnetic quantum number of the excited state and $m_{\rm g}$ is the magnetic quantum number of the ground nuclear state). Besides, non-resonant electronic radiation and nuclear resonant radiation are specularly reflected, maintaining the π-polarized state.

The susceptibility ($\chi_{\rm d}$) consists of an electron and two nuclear scattering amplitudes and is given by

$$\begin{aligned}\chi_{\rm d}(E) &= \chi_{\rm e} + \chi_{\rm n} \\ &= (\lambda^2/\pi V_0)\left[f^{\rm e} + f^{\rm n}_{1/2,1/2}\left(E, E_{1/2,1/2}\right)\right. \\ &\quad \left. + f^{n}_{-1/2,-1/2}\left(E, E_{-1/2,-1/2}\right)\right],\end{aligned} \tag{3}$$

where $f^{\rm e}$ and $f^{n}_{m_{\rm e},m_{\rm g}}$ represent the electronic scattering amplitude and the nuclear resonant scattering amplitude for $\Delta m = m_{\rm e} - m_{\rm g}$, respectively. λ, V_0 and $E_{m_{\rm e},m_{\rm g}}$ represent the

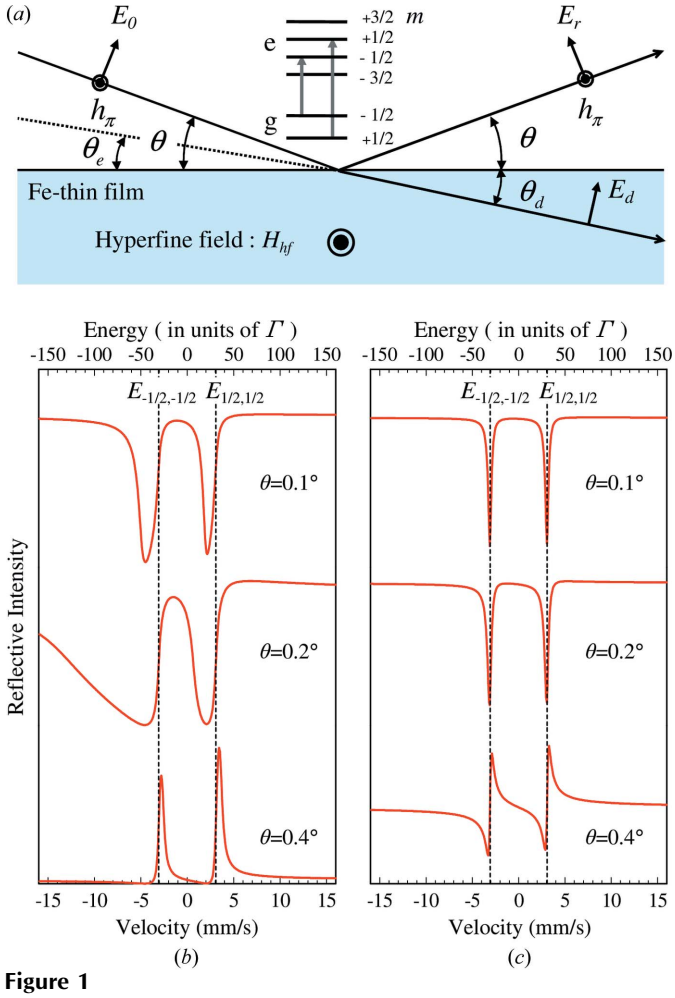

Figure 1
(*a*) Assumed sample condition. (*b*, *c*) Calculated GIMS spectra for $\Delta m = 0$ transitions of the ferromagnetic iron thin films. The ^{57}Fe isotope enrichment is (*b*) 95% and (*c*) 2.17%. In the graphs the horizontal axis is the energy of the incident beam. According to the custom in Mössbauer spectroscopy, the *x*-axis is shown as the velocity, whose zero corresponds to the centre of the sextet of α-Fe (lower horizontal axis). For the reader's convenience, this axis is also shown as the energy in units of the natural line width of the ^{57}Fe nuclear resonance, Γ (upper horizontal axis).

wavelength, unit-cell volume and nuclear resonance energy for $\Delta m = m_e - m_g$.

For ideal α-Fe and 14.4 keV radiation, electron and nuclear susceptibilities are given by

$$\chi_e \cong (-14.6 + 0.7i) \times 10^{-6}, \quad (4)$$

$$\chi_n = -\frac{3\lambda^3 N \eta C^2 f_{LM}}{8\pi^2 V_0 (1+\alpha)} \times \left[\left(\frac{E - E_{1/2,1/2}}{\Gamma/2} + i\right)^{-1} + \left(\frac{E - E_{-1/2,-1/2}}{\Gamma/2} + i\right)^{-1}\right]. \quad (5)$$

The electronic susceptibility is the same value as used in a previous study (Andreeva *et al.*, 1996). The parameters for nuclear susceptibility are given in Table 1.

Figs. 1(*b*) and 1(*c*) show the calculations on the energy- and incidence-angle-dependence of GIMS spectra of ^{57}Fe-enriched ($\eta = 0.95$) and non-enriched ($\eta = 0.0217$, natural abundance) films.

Table 1
Parameters used in the theoretical calculations.

Energy of ^{57}Fe nuclear resonance	$E_0 = 14.4125$ keV
Wavelength corresponding to E_0	$\lambda_0 = 0.8602$ Å
Unit-cell volume of α-Fe	$V_0 = 23.6399$ Å^3
Number of Fe atoms per unit cell	$N = 2$
Relative abundance of ^{57}Fe nuclei	$\eta = 0.95$ (enriched) or 0.0217 (non-enriched)
Internal conversion coefficient	$\alpha = 8.21$
Widths of resonant lines	$\Gamma = 0.1$ mm s^{-1}
Clebsch–Gordan coefficients for $\Delta m = 0$	$C_{\Delta m=0} = (2/3)^{1/2}$
Lamb–Mössbauer factor	$f_{LM} = 0.7$
Relation between energy and velocity	$E = E_0 (1 + v/c)$
Velocity of light	$c = 2.998 \times 10^8$ m s^{-1}

In the case of ^{57}Fe-enriched film, as shown in Fig. 1(*b*), all calculated spectra clearly show the coherent interference effects between the three scatterings, *i.e.* the electronic scattering and the two allowed nuclear scatterings for $\Delta m = 0$ transitions. This is because the nuclear susceptibility (χ_n) at resonance energies becomes comparable with the electronic one (χ_e). At a small incident angle ($\theta = 0.1°$) below the critical angle of the electronic total reflection ($\theta_e \simeq 0.22°$), the spectrum shows noticeable asymmetries. The absorption dips are shifted towards lower energies than the exact nuclear resonant energies for $\Delta m = 0$ transitions of α-Fe. As discussed by Bernstein & Campbell (1963), the shift is caused by the interference of nuclear and electronic scatterings: the real part of the susceptibility (χ_d) varies from negative to positive values at an energy slightly lower than the nuclear resonance energy. Besides, the interference between two nuclear transitions lowers the minimum of the absorption dip at the lower nuclear resonance energy ($E_{-1/2,-1/2}$) from that of the absorption dip at the higher nuclear resonance energy ($E_{1/2,1/2}$). The interference of nuclear and electronic scatterings is more remarkable around the critical angle, owing to the rapid reduction of the contribution of χ_e to the reflectivity. Actually, at $\theta = 0.2°$ ($\sim\theta_e$), the calculated spectrum shows a marked deformation, reflecting a strong interference effect of nuclear and electronic scatterings. Note that the specular reflectivity of the nuclear resonant γ-rays is maintained even at angles greater than θ_e because the number of nuclear resonant ^{57}Fe atoms in the iron film is increased by a large penetration depth of X-rays. Finally, at an angle greater than θ_e ($\theta = 0.4°$), the specular reflection is dominated by the channel of nuclear scattering. Consequently, the spectrum shows what is called 'pure nuclear total reflection', whose peaks are slightly shifted towards higher energies than the exact resonant energies of ^{57}Fe in α-Fe; the real part of the susceptibility is at its maximum negative at the shifted peak energies (Isaenko *et al.*, 1994).

In the case of non-enriched film, the electronic susceptibility (χ_e) is sufficiently larger than the nuclear susceptibility (χ_n). Therefore, at $\theta < \theta_e$, the reflectivity is dominated by the channel of electronic scattering, and thus the coherent interference effects become negligible. Such a unique nature is shown in the spectrum of $\theta = 0.1°$ [see Fig. 1(*c*)]. The calcu-

lation clearly shows spectra similar to the conventional RIMS absorption profile: the energy of the absorption dips is completely in agreement with the resonant energies for $\Delta m = 0$ nuclear transitions of α-Fe. As shown in the spectrum of $\theta = 0.2^\circ$, the interference effect is still fairly weak even at an angle slightly lower than θ_e. These results suggest that the GIMS of dilute ^{57}Fe in the mirror-like film, measured at the low grazing-incident angles ($<\theta_e$), is virtually the same as the Mössbauer transmission measurement. On the other hand, at $\theta > \theta_e$, the comparable contribution of nuclear and electronic scatterings to the spectrum is observed dramatically. As shown in the spectrum of $\theta = 0.4^\circ$, the calculated profile shows a rapid fall and a steep peak in the vicinity of two nuclear resonance energies, whose origins are the destructive and constructive interference between nuclear and electronic scatterings. Note that, in the ^{57}Fe non-enriched case, the GIMS spectra scarcely show the interference between different nuclear transitions and the real part of the susceptibility (χ_d) is always of negative sign. These features are useful to the applied research because the simple spectral profiles allow us to perform a detailed data analysis for the complicated HF structure. In the following sections we describe the E-GIMS experiments with SR-^{57}Fe-Mössbauer radiation, which includes the basic studies of E-GISRMS for dilute ^{57}Fe in mirror-like films.

3. Experimental procedures

The experiments were performed at beamline BL11XU of SPring-8. The electron current of the storage ring was kept at 100 mA at 8.0 GeV. The experimental set-up is schematically shown in Fig. 2. A Si (111) double-crystal monochromator cooled by liquid nitrogen was used to handle the high heat load of undulator radiation (Shiwaku *et al.*, 2004). The σ-polarized incident X-rays were monochromated to a bandwidth of 2.5 meV at a 14.4 keV resonance energy of ^{57}Fe nuclei by a high-resolution monochromator consisting of asymmetric Si (511) and asymmetric Si (975) channel-cut crystals (Mitsui

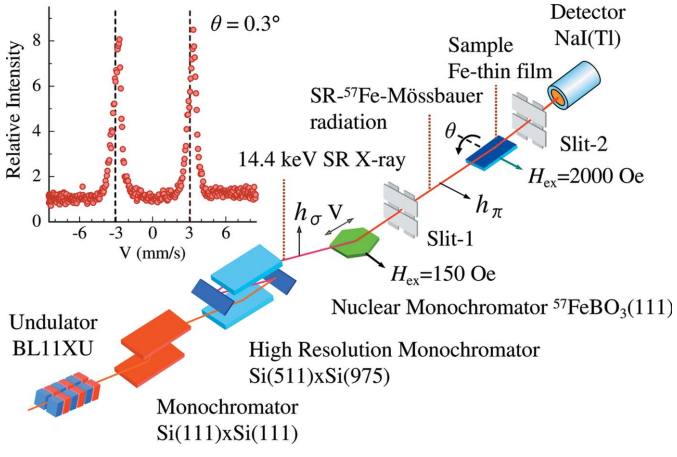

Figure 2
Experimental optics and pure nuclear total reflection from a 100 nm-thick 95% ^{57}Fe-enriched thin film measured at $\theta = 0.3^\circ$. Dashed lines in the graph are the nuclear resonant energies for $\Delta m = 0$ transitions of bulk α-Fe.

et al., 2001). The X-rays were incident on the recently developed variable-frequency NBM (Mitsui *et al.*, 2009). The π-polarized SR-^{57}Fe-Mössbauer radiation with a narrow bandwidth of 15.4 neV was produced by a pure nuclear Bragg reflection from ^{57}Fe 95%-enriched $^{57}FeBO_3$(111) kept near the Néel point (348.8 K) in an external field of 150 Oe (Mitsui *et al.*, 2009). The nuclear resonance energy of the NBM was changed by the Doppler effect with the crystal oscillating parallel to the (111) plane in a sinusoidal velocity mode at 10 Hz. Behind slit-1, the peak photon flux was 1.8×10^4 s^{-1}, the beam size was 0.3 mm (V) $\times$ 1.6 mm (H), the divergence was 15 arcsec (H) $\times$ 3 arcsec (V) and the noise level was below 3.0%. After slit 1, the SR-^{57}Fe-Mössbauer radiation was incident on the surface of the thin film at some grazing angles of θ; behind slit 2 the specularly reflected photons were counted by a NaI scintillation detector.

In the present experiments, isotope-enriched (^{57}Fe, 95%) and natural-abundance (^{57}Fe, 2.17%) 100 nm-thick iron films were prepared to study the basic features of E-GIMS. In addition, Cr/Fe multilayer films [^{56}Fe(10 $-$ d nm)/^{57}Fe(0.2 nm)/^{56}Fe(d nm)/Cr(1.0 nm): d = 0.0, 2.0] were also prepared to demonstrate the E-GIMS measurement using the ^{57}Fe-probe layer technique. These films were epitaxically grown using an MBE machine on an MgO (001) substrate with a Cr (1 nm) buffer layer.

4. Experimental results and discussion

Firstly, as a performance study of E-GISRMS with SR-^{57}Fe-Mössbauer radiation, a 100 nm-thick 95% ^{57}Fe-enriched iron thin film was measured at a high grazing angle of $\theta = 0.3^\circ$. The sample size was 5 $\times$ 30 $\times$ 0.5 mm (width $\times$ length $\times$ thickness). To selectively excite two nuclear transitions of $\Delta m = 0$, the HF field of ^{57}Fe nuclei in the film was aligned parallel to the magnetic unit vector of π-polarized incident SR-^{57}Fe-Mössbauer radiation by the external field of 2 kOe. In this way the optical system offers an ideal experimental condition for the direct observation of the E-GIMS spectrum calculated in the previous section. The room-temperature E-GISRMS spectrum measured at $\theta = 0.3^\circ$ is shown in the upper left side of Fig. 2. The two resonant scattering peaks corresponding to the $\Delta m = 0$ nuclear transitions are observed clearly. These reflection peaks are associated with the pure nuclear total reflection; the specular reflection at $\theta = 0.3^\circ$ ($>\theta_e$) leads to a strong suppression of the electronic scattering and is governed by the contribution of much larger nuclear scattering. In the present study the statistically sufficient spectrum was obtained with a very short measurement time of 10 min. The result proves an outstanding potential of E-GISRMS with SR-^{57}Fe-Mössbauer radiation because the typical data collection time of a GIMS spectrum with a ^{57}Co source is several days or more. Because of the excellent visibility, one can see clearly that the scattering peaks are slightly shifted to the right of the nuclear resonant energies for $\Delta m = 0$ transitions of α-Fe. This result is qualitatively consistent with the calculated spectrum at high grazing angle ($\theta > \theta_e$) in Fig. 1(*b*).

Secondly, a 100 nm-thick ^{57}Fe non-enriched thin film was measured to verify the theoretical predictions on the GIMS spectrum for the natural abundance case. The sample size was 5 × 18 × 0.5 mm (width × length × thickness). The room-temperature E-GISRMS spectra measured at three different grazing angles are shown in Figs. 3(*a*)–3(*c*). As discussed in the previous section, the spectrum at a small grazing angle of θ = 0.16° ($<\theta_e$) clearly shows the conventional MS absorption profile with no significant coherent interference effect. The spectrum can be well fitted with Lorentzian curves, whose minimum coincides precisely with the resonance energy positions of α-Fe [see the dashed lines in Fig. 3(*a*)]. On the other hand, as shown in Figs. 3(*b*) and 3(*c*), the E-GISRMS spectra measured near the critical angle show clear asymmetric shapes, corresponding to the coherent interference between the electronic and nuclear scatterings. Since the electronic contribution to the specular reflectivity is rapidly reduced near the critical angle, the asymmetric feature of the spectrum is drastically enhanced by the slight increase in grazing angles from θ = 0.20°($<\theta_e$) to θ = 0.23°($>\theta_e$). The overall behaviours of the observed E-GISRMS spectra are in good agreement with the theoretical results [see Fig. 1(*c*)]. As indicated by the arrows in Fig. 3(*c*), the reflectivity minima and maxima positions coincide with the theoretically calculated positions for θ = 0.23°. The results are the first direct evidence of the incidence angle dependence of the E-GIMS spectrum for the ^{57}Fe non-enriched iron thin film.

In particular, as a most remarkable optical phenomenon, we should pay attention to the fact that the E-GISRMS of thin films with low ^{57}Fe content can yield a conventional Mössbauer absorption spectrum in the low-angle region ($\theta < \theta_e$). As has already been pointed out in the theoretical section, this spectral feature makes it easy to analyze the local magnetic states composed of complicated HF interactions. Such a measurement was demonstrated by the local Mössbauer analysis in Cr/Fe epitaxial thin films on MgO (001), containing 1 ML-thick (ML = monolayer) ^{57}Fe probe atoms.

Fig. 4(*a*) shows the prepared Cr/Fe multilayer structures of MgO(001)/Cr(1.0 nm)/^{56}Fe(10 − *d* nm)/^{57}Fe(0.2 nm)/^{56}Fe(*d* nm)/Cr(1.0 nm). Since the probe layer consisting of 0.2 nm (∼1.0 ML) ^{57}Fe is separated from the upper Cr/Fe interface by a *d* nm intercalating spacer layer of non-resonant ^{56}Fe isotope, the measured Mössbauer spectrum can offer information on the surface/interface features with 1 ML sensitivity. The room-temperature E-GISRMS spectra were measured for two different *d* values (*d* = 2.0 and 0.0) at low grazing angle (θ = 0.16° < θ_e). In Fig. 4(*a*) the π-polarized Mössbauer beam was incident on the thin film with and without external magnetic field (H_{ex}). Here, the penetration depth (D_p) of X-rays under the electronic total reflection condition was estimated to be a few nanometers, which was a bit deeper than the ^{57}Fe probe layer position in the thin films [see Fig. 4(*a*)]. In this case the nuclear contribution to the reflectivity became negligible because of the relatively low ^{57}Fe content, so that the reflectivity was mainly determined by the contribution of much larger electronic scattering, as previously discussed for E-GISRMS of ^{57}Fe non-enriched film. The E-GISRMS spectra without external field were measured with a data collection time of 4.0 h. The results for the two different *d* values are shown in Figs. 4(*b*) and 4(*c*).

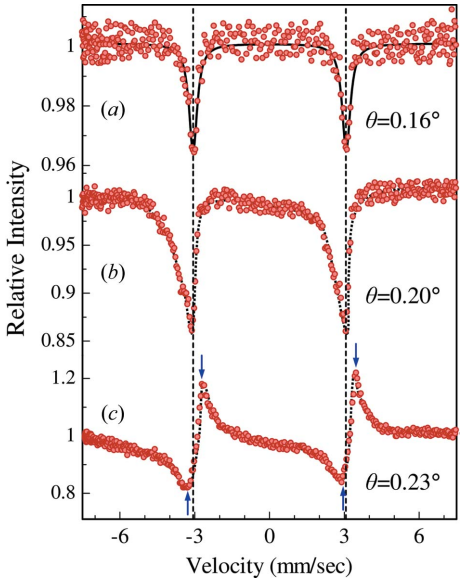

Figure 3
E-GISRMS spectra from a 100 nm-thick ^{57}Fe non-enriched thin film measured at different incidence angles: (*a*) θ = 0.16°, (*b*) θ = 0.20°, (*c*) θ = 0.23°. Dashed lines are the nuclear resonant energies for Δm = 0 transitions of bulk α-Fe. The solid line is the Lorentzian fit curve. Dotted lines are guides for the eye. The four arrows show the theoretically predicted reflectivity minima and maxima positions for the spectrum of θ = 0.23°.

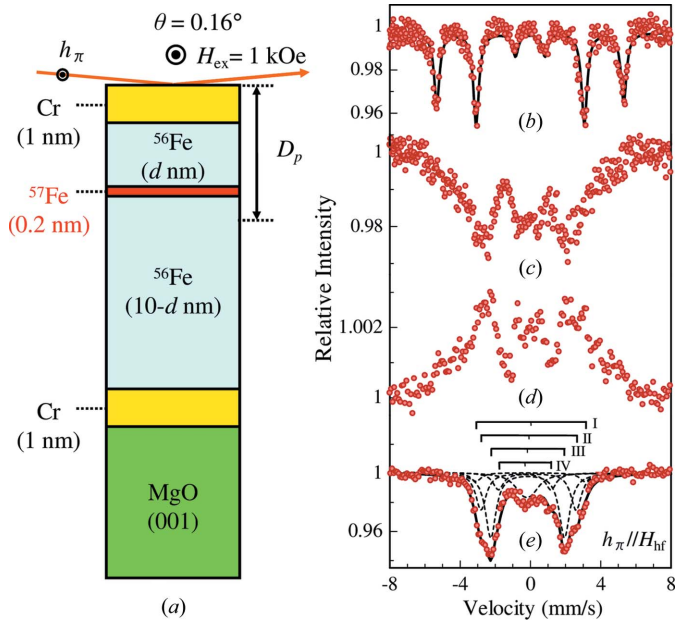

Figure 4
(*a*) Principal structure of the prepared Cr/Fe films and (*b*), (*c*) E-GISRMS spectra without external field: the distance between the Cr/Fe interface and the ^{57}Fe probe layer is (*b*) *d* = 2 nm, (*c*) *d* = 0 nm. (*d*) CEMS spectrum for the Cr/Fe film of *d* = 0. (*e*) E-GISRMS spectra for the Cr/Fe film of *d* = 0 with external field (h_π // H_{ex}). The solid line corresponds to the fitting of the spectrum. Dashed lines represent subspectra related to the different HF fields near the Cr/Fe interface.

As shown in Fig. 4(*b*), the spectrum for d = 2.0 nm shows typical magnetic sextet lines of bulk α-Fe (H_{hf} = 33 T). The relative line intensities of (3:4:1:1:4:3) indicates random in-plane magnetization of the film, according to the polarization dependence of the nuclear resonant scattering amplitude (Bernstein & Campbell, 1963). Note that the ratio (3:4:1:1:4:3) coincides with that of the conversion electron MS (CEMS) of the in-plane magnetized iron film; the CEMS measurement is usually performed by unpolarized 14.4 keV Mössbauer γ-rays, whose beam direction is perpendicular to the film plane. In contrast, as shown in Fig. 4(*c*), the spectrum for d = 0 clearly shows a complex HF structure induced at the Cr/Fe interface. It is clear at a glance that the profile is formed by the superposition of several magnetically split subspectra, whose main components have considerably different HF fields, whose magnitude is less than that of bulk α-Fe. The profile, lacking the bulk-like spectral component, confirms that the interface-sensitive E-GISRMS spectrum is obtained successfully. As a reference, a CEMS spectrum for d = 0 without the external field was also measured by using a ^{57}Co source with an activity of 46 mCi [see Fig. 4(*d*)]. The data collection time was one week, which was much longer than that of the E-GISRMS. As expected, there is an excellent horizontal symmetry between the E-GISRMS and CEMS spectral profiles as shown in Figs. 4(*c*) and 4(*d*). These results demonstrate clearly that E-GISRMS can present information on the HF interactions of a 1 ML-thick ^{57}Fe probe layer in a very short measurement time compared with the CEMS with RI source. Note that the RI-based CEMS spectrum for a few monoloayer ^{57}Fe probe atoms at the Cr/Fe interface can be obtained in a few days but it is dominated by the distributed bulk-like HF fields because of the contribution from the second and third ^{57}Fe atomic layers. These layers often make it difficult to characterize the intrinsic interface effects on the HF interactions.

Nevertheless, in Figs. 4(*c*) and 4(*d*) precise data analysis is rather difficult because these spectra have many absorption lines. To simplify the spectrum, as shown in Fig. 4(*a*), the E-GISRMS spectrum for d = 0 was measured with an external field (H_{ex} = 1 kOe); the HF fields in the thin film were aligned parallel to the magnetic polarization unit vector h_π of the π-polarized incident MS beam. Consequently, as shown in Fig. 4(*e*), the only two nuclear transitions of Δm = 0 were excited selectively so that the number of the absorption lines were decreased significantly. The data collection time of this spectrum was 5.0 h. The measured spectrum can be fitted well with a superposition of four magnetically split subspectra (I)–(IV) and a paramagnetic-like subspectrum (at the centre). The four subspectra (I)–(IV) show HF fields of 33.0, 29.1, 22.5 and 16.0 T. In analogy to work with a thicker probe layer using a RI source (Landes *et al.*, 1990), the HF fields of 29.1, 22.5 and 16.0 are due to the step structures of the interface; the Cr/Fe interface is composed of flat regions separated by step sites on a scale of a few monolayers so that the magnetic HF field at the ^{57}Fe nuclei is reduced by the increase of neighbouring Cr atoms, which leads to the spin transfer from Fe to Cr. At the same time the isomer shift values (centre of subspectra) gradually decrease in going from subspectrum (II) to subspectrum (IV). This behaviour is also consistent with the result of increasing number of Cr neighbours, which leads to a higher *s*-electron density at the Fe nucleus (Dubiel & Zukrowski, 1981; Maksymowicz, 1982). On the other hand, the bulk-like ($H_{hf} \simeq 33$ T) and paramagnetic-like components may be attributed to ^{57}Fe atoms diffused into the Fe or Cr layers, respectively. These results demonstrate that the combination of E-GISRMS and the 1 ML-thick ^{57}Fe probe layer technique is a useful tool for the atomic-scale characterization for highly complex thin films and interface structures.

5. Conclusion

In this study E-GISRMS with a NBM has been investigated for performing surface investigations. Calculations and experiments for ^{57}Fe-enriched (95%) and non-enriched (2.17%) iron thin films have elucidated coherent interference effects between electronic and nuclear scattering channels in the specular reflection of ^{57}Fe-Mössbauer radiation. A new surface/interface-sensitive method has also been developed by combining E-GISRMS under non-interference conditions with the ^{57}Fe probe layer technique. This approach gives rise to the conventional MS absorption spectrum with atomic-scale depth resolution, which provides quite new possibilities for MS analysis on complex magnetic thin films. The high-brilliant SR ^{57}Fe-Mössbauer radiation enables E-GIMS measurement in a short measurement time and the pure linear polarized beam simplifies the spectral profile of E-GISRMS *via* the selective excitation of nuclear transitions. The simple optical system is suitable for applied research under special conditions, such as low temperatures, high magnetic fields and *in situ* measurement with various gas environments. As a special advantage, the developed method is available even for the SR bunch modes unsuitable for SRMS using a time-gating method. On the other hand, E-GISRMS with a NBM still has the restriction that it is inapplicable to the measurement for various Mössbauer isotopes other than the ^{57}Fe nucleus. In future studies, advantages and disadvantages of the GISRMS, using NFS, SD or NBM, will become more clear. Eventually the complementary use of three types of GISRMS and CEMS will offer unique insights into the magnetic structures at the surface and/or interface of various advanced functional thin films, such as magnetic tunnel junctions, spin valves and spin injection structures.

The authors thank Professor S. Kikuta for his worthwhile comments. The present work was supported by the Core Research for Evolutional Science and Technology (CREST) project of the Japan Science and Technology Agency. KM also thanks the Japan Society for the Promotion of Science for financial support from a Grant-in-Aid for Scientific Research (C).

References

Andreeva, M. A., Irkaev, S. M. & Semenov, V. G. (1996). *Hyperfine Interact.* **97/98**, 605–623.

Baron, A. Q. R., Arthur, J., Ruby, S. L., Brown, D. E., Chumakov, A. I., Smirnov, G. V., Brown, G. S. & Salashchenko, N. N. (1992). Contribution to the *International Conference on Anomalous Scattering*, Malente, Germany. Unpublished.

Bernstein, S. & Campbell, E. C. (1963). *Phys. Rev.* **132**, 1625–1633.

Callens, R., Coussement, R., L'abbé, C., Nasu, S., Vyvey, K., Yamada, T., Yoda, Y. & Odeurs, J. (2002). *Phys. Rev. B*, **65**, 180404.

Chumakov, A. I., Niesen, L., Nagy, D. L. & Alp, E. E. (1999). *Hyperfine Interact.* **123**/**124**, 427–454.

Deák, L., Bottyán, L., Callens, R., Coussement, R., Major, M., Serdons, I. & Yoda, Y. (2006). *Hyperfine Interact.* **167**, 709–715.

Dubiel, S. M. & Zukrowski, J. (1981). *J. Magn. Magn. Mater.* **23**, 214–228.

Hastings, J. B., Siddons, D. P., van Bürck U, Hollatz, R. & Bergmann, U. (1991). *Phys. Rev. Lett.* **66**, 770–773.

Irkaev, S. M., Andreeva, M. A., Semenov, V. G., Belozerskii, G. N. & Grishin, O. V. (1993*a*). *Nucl. Instrum. Methods Phys. Res. B*, **74**, 545–553.

Irkaev, S. M., Andreeva, M. A., Semenov, V. G., Belozerskii, G. N. & Grishin, O. V. (1993*b*). *Nucl. Instrum. Methods Phys. Res. B*, **74**, 554–564.

Irkaev, S. M., Andreeva, M. A., Semenov, V. G., Belozerskii, G. N. & Grishin, O. V. (1995). *Nucl. Instrum. Methods Phys. Res. B*, **103**, 351–358.

Isaenko, S. A., Chumakov, A. I. & Shinkarev, S. I. (1994). *Phys. Lett.* A**186**, 274–278.

Kikuta, S. (1992). Contribution to the *International Conference on Anomalous Scattering*, Malente, Germany. [The article was published in *X-ray Resonant (Anomalous) Scattering*, edited by G. Materlik, C. J. Sparks and K. Fischer (1994), p. 63. Amsterdam: Elsevier.]

L'abbé, C., Meersschaut, J., Sturhahn, W., Jiang, J. S., Toellner, T. S., Alp, E. E. & Bader, S. D. (2004). *Phys. Rev. Lett.* **93**, 037201.

Landes, J., Sauer, Ch., Brand, R. A., Zinn, W., Mantl, S. & Kajcsos, Zs. (1990). *J. Magn. Magn. Mater.* **86**, 71–77.

Maksymowicz, A. Z. (1982). *J. Phys. F*, **12**, 537–548.

Mitsui, T., Hirao, N., Ohishi, Y., Masuda, R., Nakamura, Y., Enoki, H., Sakaki, K. & Seto, M. (2009). *J. Synchrotron Rad.* **16**, 723–729.

Mitsui, T., Kitao, S., Zhang, X. W., Marushita, M. & Seto, M. (2001). *Nucl. Instrum. Methods Phys. Res. A*, **467**–**468**, 1105–1108.

Nagy, D. L., Bottyán, L., Croonenborghs, B., Deák, L., Degroote, B., Dekoster, J., Lauter, H. J., Lauter-Pasyuk, V., Leupold, O., Major, M., Meersschaut, J., Nikonov, O., Petrenko, A., Rüffer, R., Spiering, H. & Szilágyi, E. (2002). *Phys. Rev. Lett.* **88**, 157202.

Planckaert, N., Callens, R., Demeter, J., Laenens, B., Meersschaut, J., Sturhahn, W., Kharlamova, S., Temst, K. & Vantomme, A. (2009). *Appl. Phys. Lett.* **94**, 224104.

Röhlsberger, R., Bansmann, J., Senz, V., Jonas, K. L., Bettac, A. & Meiwes-Broer, K. H. (2003). *Phys. Rev. B*, **67**, 245412.

Röhlsberger, R., Thomas, H., Schlage, K., Burkel, E., Leupold, O. & Rüffer, R. (2002). *Phys. Rev. Lett.* **89**, 237201.

Seto, M., Masuda, R., Higashitaniguchi, S., Kitao, S., Kobayashi, Y., Inaba, C., Mitsui, T. & Yoda, Y. (2009). *Phys. Rev. Lett.* **102**, 217602.

Shiwaku, H., Mitsui, T., Tozawa, K., Kiriyama, K., Harami, T. & Mochizuki, T. (2004). *AIP Conf. Proc.* **705**, 659–662.

Sladecek, M., Sepiol, B., Kaisermayr, M., Korecki, J., Handke, B., Thiess, H., Leupold, O., Rüffer, R. & Vogl, G. (2002). *Surf. Sci.* **507**–**510**, 124–128.

Ślęzak, T., Łaźewski, J., Stankov, S., Parlinski, K., Reitinger, R., Rennhofer, M., Rüffer, R., Sepiol, B., Ślęzak, M., Spiridis, N., Zając, M., Chumakov, A. I. & Korecki, J. (2007*b*). *Phys. Rev. Lett.* **99**, 066103.

Ślęzak, T., Ślęzak, M., Matlak, K., Röhlsberger, R., L'ábbe, C., Rüffer, R., Spiridis, N., Zając, M. & Korecki, J. (2007*a*). *Surf. Sci.* **601**, 4300–4304.

Ślęzak, T., Ślęzak, M., Zajac, M., Freindl, K., Kozioł-Rachwał, A., Matlak, K., Spiridis, N., Wilgocka-Slezak, D., Partyka-Jankowska, E., Rennhofer, M., Chumakov, A. I., Stankov, S., Rüffer, R. & Korecki, J. (2010). *Phys. Rev. Lett.* **105**, 027206.

Smirnov, G. V., van Bürck, U., Chumakov, A. I., Baron, A. Q. R. & Rüffer, R. (1997). *Phys. Rev. B*, **55**, 5811–5815.